Superconductivity in multiorbital systems with repulsive interactions: Hund's pairing versus spin-fluctuation pairing

Mercè Roig [1], Astrid T. Rømer,[1] Andreas Kreisel [2], P. J. Hirschfeld,[3] and Brian M. Andersen[1]

[1]*Niels Bohr Institute, University of Copenhagen, 2100 Copenhagen, Denmark*
[2]*Institut für Theoretische Physik, Universität Leipzig, D-04103 Leipzig, Germany*
[3]*Department of Physics, University of Florida, Gainesville, Florida 32611, USA*

Hund's pairing refers to Cooper pairing generated by onsite interactions that become attractive due to large Hund's exchange J. This is possible in multiorbital systems even when all local bare interactions are repulsive, since attractions in specific channels are given by certain linear combinations of interaction parameters. On the other hand, pairing processes such as the exchange of spin fluctuations are also present. We compare mean-field Hund's pairing and spin-fluctuation-mediated pairing using electronic bands appropriate for different classes of multiorbital systems over a wide range of interaction parameters. We find that, for systems without clear nesting features, the superconducting state generated by the Hund's mechanism agrees well with that from the full fluctuation exchange vertex when Hund's exchange and spin-orbit coupling are sufficiently large. On the other hand, for systems characterized by a peaked finite-momentum particle-hole susceptibility, spin-fluctuation pairing generally dominates over Hund's pairing. From this perspective Hund's pairing states appear unlikely to be realized in systems like Sr_2RuO_4 and generic iron-based superconductors.

I. INTRODUCTION

The problem of creating superconductivity in systems where local interactions are repulsive dates back to Kohn and Luttinger, who studied how the screened Coulomb interaction can give rise to effective attraction in higher angular momentum channels in the electron gas [1]. Electrons binding in such pair states can avoid the Coulomb energy cost largely without the need of retardation in time, since the pair wave function has a node at the origin. In the electron gas, as in single-band lattice systems like the Hubbard model, the bare interaction itself cannot pair directly. Instead, one needs to calculate the effective interaction, i.e., sum screening processes leading to Friedel oscillations that allow for attraction in certain channels [1–8].

By contrast, many unconventional superconductors of current interest involve electrons in multiple bands at the Fermi level, subject to strong local Coulomb repulsion [9]. This situation is described by a Hubbard-Kanamori Hamiltonian, with Hund's exchange J, inter-orbital Coulomb interaction U', and pair hopping term J' in addition to the usual intraorbital Hubbard U. In this model, the attraction binding electrons into Cooper pairs can arise in different ways. First, it can be generated as in the one-band case by summing the pair scattering processes. In the iron-based superconductors, magnetic fluctuations connecting the Fermi surface pockets in the Brillouin zone (BZ) are thought to be exchanged, leading to dominant spin-singlet sign-changing $s_{\pm}$- or d-wave condensates [10–12].

In recent years, a qualitatively different route to pair formation in multiorbital models with local repulsive interactions has been explored by a number of authors [13–26]. Projecting onto appropriate symmetry channels, the interaction parameters U, U', J, J' appear in certain combinations that may be negative and lead to direct attraction. For example, for certain iron-based systems, an interorbital spin-triplet state is stabilized by an interaction channel proportional to $U' - J$, providing attraction when J exceeds U' [23] and spin-orbit coupling (SOC) is present to generate a Cooper logarithm at the instability [16,23]. We refer to pairing of this type as "Hund's pairing" since it requires a large Hund's exchange J. It has been suggested to produce exotic pair states in uranium-based superconductors [14–16], iron-based superconductors [22–24], and Sr_2RuO_4 [16–20].

Even if Hund's pairing states are stable, they still "compete" with more usual spin-fluctuation-driven pairing states [27]. Until now, no one has compared the two types of pairing on an equal footing. This is important because, although SOC creates a logarithmic instability, the corresponding T_c may be very low because of the small weight of intra-band pairing present at the Fermi surface. One expects that for sufficiently large J and SOC such states will indeed be stable, but can Hund's pairing outcompete spin-fluctuation driven pairing, or will the latter states remain favorable also at large J/U? And how might this depend on the underlying band structure? It is vital that the discussion regarding these candidate states in systems of current interest proceed with accurate estimates of their true viability.

In this work, we compare the superconducting order obtained from the two different pairing mechanisms: local Hund's pairing at the mean-field level vs spin-fluctuation mediated pairing. The comparative study is performed for

two very different multiorbital systems: (1) a two-orbital model forming two Γ-centered Fermi pockets [23], and (2) a three-orbital model relevant for Sr_2RuO_4 [28,29]. In both procedures, we determine the gap structure and T_c while exploring different interaction regimes, varying U, J/U, and the value of SOC λ_{so}. As is well-known, Hund's pairing at the mean-field level is only operative in the regime, $J > U'$ [18,23]. This criterion can be renormalized by higher-order processes [16,30], effectively expanding the "Hund's regime." We find that, inside this regime, pairing driven by Hund's coupling agrees almost quantitatively with spin-fluctuation pairing when the electronic structure generates a susceptibility with weak momentum structure. By contrast, when the susceptibility contains sufficient momentum structure, spin-fluctuation processes generally dominate the pairing, also in the Hund's regime. We analyze this limit in detail and explain why Hund's pairing and spin-fluctuation pairing can lead to both qualitatively and quantitatively different superconducting solutions.

II. METHOD

Before applying specific band structures, we describe the methodology applied as pairing kernel for both mechanisms in question. The starting point is the multiorbital interaction

$$\hat{H}_{\text{int}} = \frac{1}{2} \sum_{\mathbf{k},\mathbf{k}'\{\tilde{\mu}\}} [V(\mathbf{k}, \mathbf{k}')]^{\tilde{\mu}_i,\tilde{\mu}_l}_{\tilde{\mu}_j,\tilde{\mu}_k} c^{\dagger}_{\mathbf{k}\tilde{\mu}_i} c^{\dagger}_{-\mathbf{k}\tilde{\mu}_j} c_{-\mathbf{k}'\tilde{\mu}_l} c_{\mathbf{k}'\tilde{\mu}_k}, \quad (1)$$

where $c_{\mathbf{k}\tilde{\mu}}$ annihilates an electron with momentum $\mathbf{k}$, and $\tilde{\mu} = (\mu, \sigma)$ is a joint index of orbital and electronic spin.

We refer to Hund's pairing when onsite interactions directly mediate superconductivity. Thus, for Hund's pairing the effective interaction of Eq. (1) is given simply by $[V(\mathbf{k}, \mathbf{k}')]^{\tilde{\mu}_i,\tilde{\mu}_l}_{\tilde{\mu}_j,\tilde{\mu}_k} = [U]^{\tilde{\mu}_i,\tilde{\mu}_l}_{\tilde{\mu}_j,\tilde{\mu}_k}$ which contain intra- (U) and interorbital Coulomb scattering (U') as well as pair-hopping terms (J, J') with the spin rotational invariant setting $U' = U - 2J$, $J' = J$; for details see the Supplemental Material (SM) [31]. We require throughout that $U' \geqslant 0$, i.e., $J/U \leqslant \frac{1}{2}$. Attractive pairing emerges when $J > U'$ (equivalently $J/U > \frac{1}{3}$) at the mean-field level, which was recently shown to generate unusual orbital-singlet, spin-triplet gap structures [16,18,20,23].

Within spin-fluctuation mediated pairing, an effective interaction is derived from random phase approximation (RPA) diagrams [9,32,33]. The pairing obtained in this framework is given by

$$[V(\mathbf{k}, \mathbf{k}')]^{\tilde{\mu}_i,\tilde{\mu}_l}_{\tilde{\mu}_j,\tilde{\mu}_k} = [U]^{\tilde{\mu}_i,\tilde{\mu}_l}_{\tilde{\mu}_j,\tilde{\mu}_k} + \left[U \frac{1}{1 - \chi_0 U} \chi_0 U \right]^{\tilde{\mu}_i,\tilde{\mu}_l}_{\tilde{\mu}_j,\tilde{\mu}_k} (\mathbf{k} + \mathbf{k}')$$
$$- \left[U \frac{1}{1 - \chi_0 U} \chi_0 U \right]^{\tilde{\mu}_i,\tilde{\mu}_k}_{\tilde{\mu}_j,\tilde{\mu}_l} (\mathbf{k} - \mathbf{k}'), \quad (2)$$

and includes, in addition to the same local interactions as the Hund's pairing scenario, explicit momentum-dependent effective interactions through the bare susceptibility $\chi_0(\mathbf{q})$; see SM for details [31]. Below we compare the two mechanisms by

solving (i) the resulting BCS gap equation

$$[\Delta_{\mathbf{k}}]^{\tilde{\mu}_i}_{\tilde{\mu}_j} = \sum_{\mathbf{k}',\tilde{\mu}_{\mathbf{k}},\tilde{\mu}_{\mathbf{l}}} [V(\mathbf{k}, \mathbf{k}')]^{\tilde{\mu}_i,\tilde{\mu}_l}_{\tilde{\mu}_j,\tilde{\mu}_k} \langle c_{-\mathbf{k}'\tilde{\mu}_l} c_{\mathbf{k}'\tilde{\mu}_k} \rangle \quad (3)$$

for different bands and interaction parameters, and (ii) analyzing the linearized gap equation (LGE) projected to band and spin space [29,31–33] to visualize the gap function $\Delta_l(\mathbf{k}_f)$ on the Fermi surface and discuss leading and subleading instabilities according to the eigenvalue λ.

III. RESULTS

A. Non-nested band structure

First, we discuss a multiorbital case with a simple band structure without nesting using the two-orbital model of Ref. [23],

$$H_0(\mathbf{k}) = \begin{pmatrix} \mu - a\mathbf{k}^2 + bk_xk_y & c(k_x^2 - k_y^2) - i\sigma\lambda_{so} \\ c(k_x^2 - k_y^2) + i\sigma\lambda_{so} & \mu - a\mathbf{k}^2 - bk_xk_y \end{pmatrix} \quad (4)$$

in the basis $[c_{\mathbf{k},xz,\sigma}, c_{\mathbf{k},yz,\sigma}]$ with the energy unit $a = 1/2m$. The Fermi surface and the momentum structure of the bare static susceptibility $\chi_0^{zz}(\mathbf{q})$ is shown in Figs. 1(a) and 1(b), respectively. At low values of $J/U < \frac{1}{3}$, the rather featureless susceptibility supports only weak (spin-fluctuation generated) superconductivity, as seen by the red curve in Fig. 1(c). The favored nature of the superconductivity in this regime is helical odd-parity pairing. By contrast, in the Hund's regime where $J/U > \frac{1}{3}$, the regime of main interest in this paper, Hund's pairing becomes active and overwhelms the helical solution, producing an interorbital spin-triplet even-parity state with an *s*-wave gap structure (in band space); see Fig. 1(d). As displayed in Fig. 1(c), spin fluctuations and Hund's pairing agree well in this case, because the onsite direct attraction dominates over the weak momentum-dependent parts of Eq. (2). Further details and parameter dependence are discussed in the SM [31]. Figure 1(e) shows the importance of nonzero λ_{so} within Hund's pairing, yielding vanishing eigenvalue for $\lambda_{so} \to 0$. Finally, Fig. 1(f) displays the T dependence of the pairing channels in orbital and spin space from Hund's pairing corresponding to the components given in Table I. The dominant A_{1g} channel $\frac{1}{2}([\Delta]^{xz\downarrow}_{yz\uparrow} + [\Delta]^{xz\uparrow}_{yz\downarrow})$ can be written as

$$(U' - J) \sum_{\mathbf{k}'} (\langle c_{-\mathbf{k}'yz\downarrow} c_{\mathbf{k}'xz\uparrow} \rangle + \langle c_{-\mathbf{k}'yz\uparrow} c_{\mathbf{k}'xz\downarrow} \rangle), \quad (5)$$

highlighting its orbital-singlet, spin-triplet structure, in agreement with earlier works [23,25]. In summary, non-nested multiorbital band structures generally exhibit agreement between the pairing strengths and gap structures obtained by Hund's pairing and spin-fluctuation pairing for $J/U > \frac{1}{3}$. However, for $J/U < \frac{1}{3}$ only the latter method enables superconductivity.

B. Nested band structure

Next, we turn to a different band representative of cases that do exhibit some nesting. We are not concerned with rare perfectly nested bands, but rather with bands exhibiting
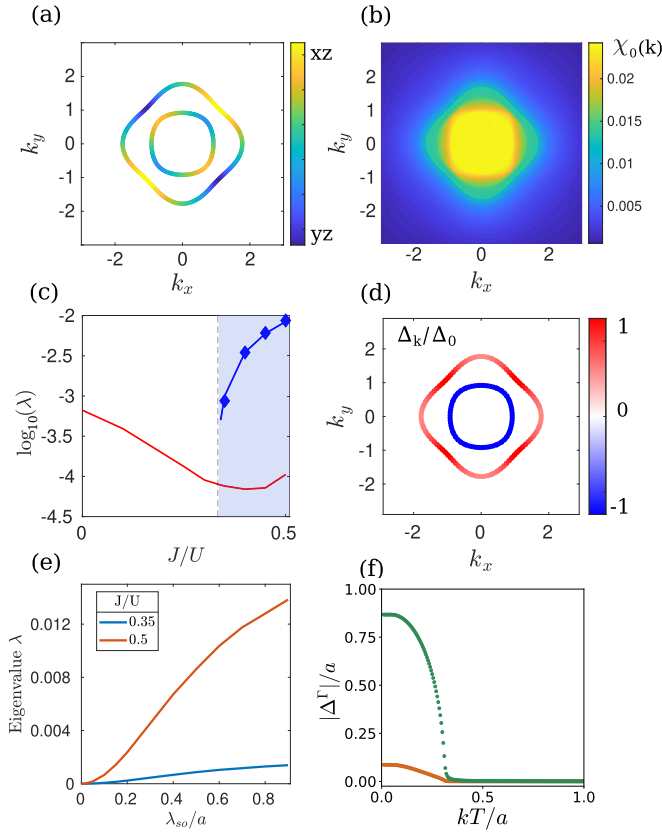
FIG. 1. (a) Fermi surface of the two-orbital model (4), with parameters $a = 1$, $b = c = \lambda_{so} = 0.5$, $\mu = 1.5$. The main orbital content is shown by the color code. (b) Momentum dependence of the static spin susceptibility $\chi_0^{zz}(\mathbf{q})$. (c) Leading eigenvalue of the LGE as a function of J/U for $U/a = 1$. Results from spin-fluctuation pairing (Hund's pairing) are indicated by solid lines (diamonds). The light blue region indicates the regime of attractive onsite Hund's pairing, $J/U > \frac{1}{3}$. (d) Superconducting gap structure (in band space) obtained at $U/a = 1$, $J/U = 0.5$, representative of all leading even-parity solutions when $J/U > \frac{1}{3}$. (e) Eigenvalue from the LGE as a function of λ_{so} for different J/U for Hund's pairing. (f) Orbital and spin structure (see Table I) from the Hund's pairing mechanism vs T for $U/a = 6$, $J/U = 0.5$, showcasing the dominant spin-triplet, orbital-singlet pairing channel (green curve) in the Hund's regime.

a degree of approximate finite-momentum nesting as typically occurs in many unconventional superconductors. As a concrete, timely example, we apply a band relevant for

TABLE I. Relevant combinations of order parameter components for the two-orbital model shown in Fig. 1 transforming as irreducible representations (IRs) of the point group D_{4h}; see also SM [31]. Orbital and spin structure are indicated by their singlet (S) or triplet (T) character.

	Channel	Orbital	Spin	IR
🟢	$\frac{1}{2}([\Delta]_{yz\uparrow}^{xz\downarrow} + [\Delta]_{yz\downarrow}^{xz\uparrow})$	S	T	A_{1g}
🟠	$\frac{1}{2}([\Delta]_{xz\downarrow}^{yz\uparrow} + [\Delta]_{xz\uparrow}^{yz\downarrow})$	T	S	A_{1g}

Sr_2RuO_4[28,29]. The normal state Hamiltonian is

$$H_0(\mathbf{k}) = \begin{pmatrix} \xi_{xz}(\mathbf{k}) & -i\sigma\lambda_{so}/2 & i\lambda_{so}/2 \\ i\sigma\lambda_{so}/2 & \xi_{yz}(\mathbf{k}) & -\sigma\lambda_{so}/2 \\ -i\lambda_{so}/2 & -\sigma\lambda_{so}/2 & \xi_{xy}(\mathbf{k}) \end{pmatrix}, \quad (6)$$

in the pseudospin basis $[c_{\mathbf{k},xz,\sigma}, c_{\mathbf{k},yz,\sigma}, c_{\mathbf{k},xy,\bar{\sigma}}]$. The dispersion relations are $\xi_{xz/yz}(\mathbf{k}) = -2t_{1/2}\cos k_x - 2t_{2/1}\cos k_y - \mu$ and $\xi_{xy}(\mathbf{k}) = -2t_3(\cos k_x + \cos k_y) - 4t_4\cos k_x\cos k_y - 2t_5(\cos 2k_x + \cos 2k_y) - \mu$ with $(t_1, t_2, t_3, t_4, t_5, \mu) = (88, 9, 80, 40, 5, 109)$ meV and atomic SOC $\lambda_{so}\mathbf{L}\cdot\mathbf{S}$, $\lambda_{so} = 20$ meV. Band parameters were chosen in ranges appropriate for Sr_2RuO_4 [28,29]. The Fermi surface is shown in Fig. 2(a), and the associated spin susceptibility with well-defined nesting peaks is displayed in Fig. 2(b). As is evident from the blue lines in Fig. 2(c), spin-fluctuation pairing generates leading even-parity nodal s' (A_{1g}) or $d_{x^2-y^2}$ (B_{1g}) gap structures throughout the entire J/U range. By s' we refer to the fact that the gap structure is nodal s wave. A subleading odd-parity helical solution (red line) is also depicted in Fig. 2(c). In the large-J region, Hund's pairing with significantly smaller eigenvalues sets in, as seen by the diamond symbols in Fig. 2(c). The critical temperatures in this regime scale as $T_c \propto e^{-1/\lambda}$ showing a dominance of spin-fluctuation mediated pairing, originating from important contributions from the fluctuation terms in the pairing kernel, Eq. (2). More details and examination of parameter dependence are given in the SM [31]

To obtain a detailed understanding of the differences between the gap structures from the two mechanisms, we turn to self-consistent solutions of the full gap equation in orbital and spin space decomposed into the appropriate irreducible representations (IRs) [34–36]. See Table II for the relevant components, and SM for the full list [31]. Focusing on the results from spin-fluctuation pairing, Figs. 2(d)–2(f) show the T dependence of the nonzero orbital channels at the large ratios $J/U = 0.3$, $J/U = 0.35$, and $J/U = 0.4$ [37]. Figure 2(d) reveals a dominant orbital-triplet, spin-singlet A_{1g} structure of the nodal s' solution (red curve) generated from spin fluctuations at $J/U = 0.3$ [29]. Inside the (mean-field) Hund's regime, i.e., for $J/U = 0.35$, the orbital-singlet spin-triplet (green curve) channel is substantial, but has not yet surpassed the orbital-triplet spin-singlet channel (red curve). As seen from the insets in Fig. 2(e), the final $T = 0$ gap structure is of the $s' + id_{x^2-y^2}$ form. This composite time-reversal symmetry broken state is expected from the LGE solutions [Fig. 2(c)] revealing that the s' and $d_{x^2-y^2}$ channels are nearly degenerate at this J/U. At even larger J/U, as seen from Fig. 2(f), spin-fluctuations favor the orbital-singlet, spin-triplet gap structure and the gap in band space becomes nodeless with sign changes between the different Fermi sheets. The solution of the gap equation within Hund's pairing is substantially simpler: the orbital structure valid throughout the regime $\frac{1}{3} < J/U < \frac{1}{2}$ is shown in Fig. 2(g) with the associated momentum gap structure displayed in the inset. In the Hund's mechanism, the orbital-singlet, spin-triplet A_{1g} channel involving interorbital pairing between xy and xz/yz orbitals dominates the pairing, as seen from Fig. 2(g). By comparing Figs. 2(f) and 2(g) it is evident that the gap structures generated by the two distinct mechanisms become similar when $J/U \simeq \frac{1}{2}$. Our
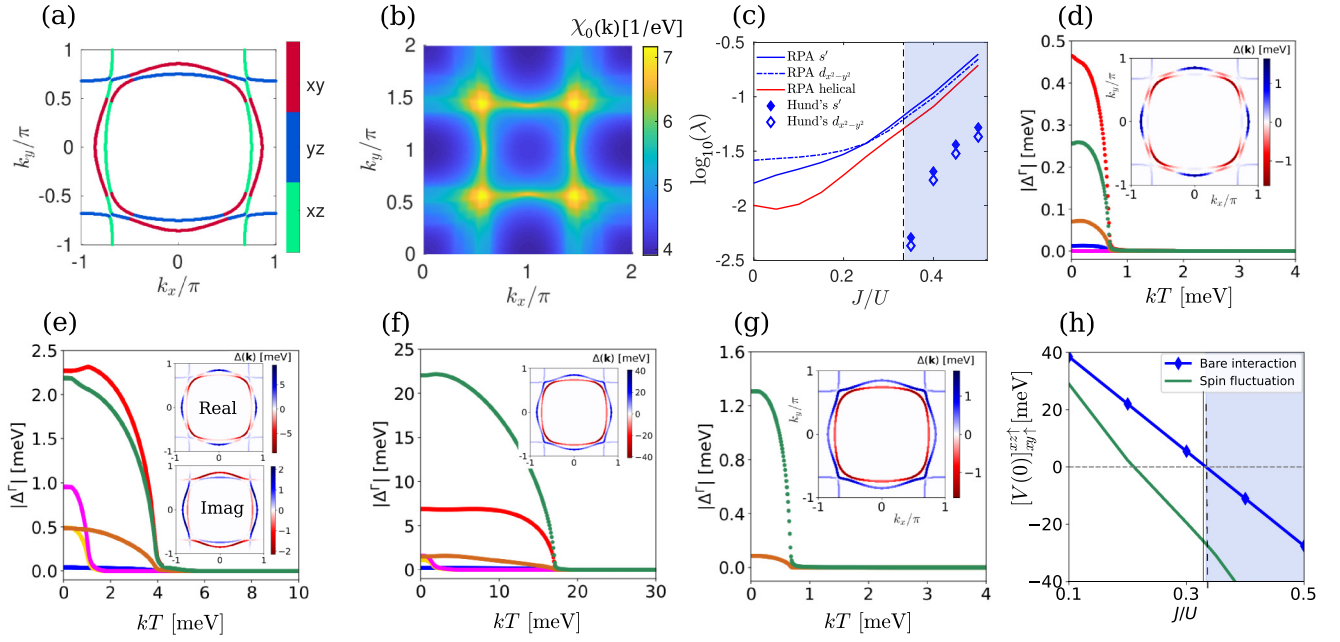
FIG. 2. (a) Fermi surface of the three-orbital model of Eq. (6). Majority orbital content is indicated by the color code. (b) Momentum dependence of the bare static susceptibility $\chi_0^{zz}(\mathbf{q})$. (c) Eigenvalues of leading and subleading solutions to the LGE, as a function of J/U for $U = 100$ meV. Spin-fluctuation (Hund's) mediated pairing is shown by lines (symbols). The shaded blue region indicates the regime of attractive Hund's pairing, $J/U > \frac{1}{3}$. (d)–(f) Orbital- and spin-structure components of the pairing gap versus T as obtained from spin-fluctuation pairing ($U = 110$ meV) for $J/U = 0.3$ (d), $J/U = 0.35$ (e), and $J/U = 0.4$ (f). See Table II for the detailed definition and color code of each channel. The insets in (d)–(g) display the gap structures on the Fermi surface. In (e) the insets represent real (top, s') and imaginary (bottom, $d_{x^2-y^2}$) parts of the leading $s' + id$ gap function at $T = 0$. (g) Orbital and spin structure of the gap as obtained from Hund's pairing with $J/U = 0.5$. Note the much smaller gap scale (and T_c) compared to (f), despite larger J/U in (g). (h) Onsite triplet-pairing component $[V(0)]_{xy\uparrow}^{xz\uparrow}$ [driving the green curves in (d)–(g)] vs J/U for spin fluctuations (green line) and Hund's pairing (blue line), revealing an enhancement of onsite attractions by spin fluctuations.

self-consistent solutions confirm, however, that even in this regime of U and J the T_c's of the Hund's pairing mechanism are substantially lower than those from spin fluctuations, in agreement with Fig. 2(c) [41].

The extent of the nominal Hund's pairing regime can be renormalized by higher-order scattering processes [16]. We demonstrate this explicitly in Fig. 2(h), displaying the J/U dependence of the dominant onsite pairing channel for (1) mean-field Hund's pairing given by $\frac{U}{2}(1 - \frac{3J}{U})$, and (2) the *onsite part* of the spin-fluctuation pairing, $V(\mathbf{r} = 0)$. For the

latter case, to second order in interactions the pairing between xz and xy-orbitals for same-spin electrons is proportional to

$$V^{(2)}(\mathbf{r} = 0) \simeq (U' - J) - UU' \sum_{\mathbf{q}} \left[\chi_0^{xz}(\mathbf{q}) + \chi_0^{xy}(\mathbf{q}) \right]$$
$$- (U')^2 \sum_{\mathbf{q}} \chi_0^{yz}(\mathbf{q}) - (U' - J)^2 \sum_{\mathbf{q}} \chi_0^{yz}(\mathbf{q}),$$

(7)

TABLE II. Same as Table I for the three-orbital model Eq. (6). We include the form factors (FF) for each channel, obtained from the projection of the gap into the different basis functions with $f_{\pm}(\mathbf{k}) = \cos 2k_x \pm \cos 2k_y$.

	Channel	FF	Orbital	Spin	IR
🔴	$\frac{1}{2\sqrt{3}}([\Delta]_{xz\downarrow}^{xz\uparrow} + [\Delta]_{yz\downarrow}^{yz\uparrow} - 2[\Delta]_{xy\downarrow}^{xy\uparrow})$	$f_+(\mathbf{k})$	T	S	A_{1g}
🔵	$\frac{1}{4}(i[\Delta]_{xy\downarrow}^{xz\downarrow} - i[\Delta]_{xy\uparrow}^{xz\uparrow} - [\Delta]_{xy\uparrow}^{yz\uparrow} - [\Delta]_{xy\downarrow}^{yz\downarrow})$	$f_+(\mathbf{k})$	S	T	A_{1g}
🟡	$\frac{1}{3}([\Delta]_{xz\downarrow}^{xz\uparrow} + [\Delta]_{yz\downarrow}^{yz\uparrow} + [\Delta]_{xy\downarrow}^{xy\uparrow})$	$f_-(\mathbf{k})$	T	S	B_{1g}
🟣	$\frac{1}{4}(i[\Delta]_{xy\downarrow}^{xz\downarrow} - i[\Delta]_{xy\uparrow}^{xz\uparrow} + [\Delta]_{xy\uparrow}^{yz\uparrow} + [\Delta]_{xy\downarrow}^{yz\downarrow})$	1	S	T	B_{1g}
🟢	$\frac{1}{4}(i[\Delta]_{xy\downarrow}^{xz\downarrow} - i[\Delta]_{xy\uparrow}^{xz\uparrow} - [\Delta]_{xy\uparrow}^{yz\uparrow} - [\Delta]_{xy\downarrow}^{yz\downarrow})$	1	S	T	A_{1g}
🟤	$\frac{1}{3}([\Delta]_{xz\downarrow}^{xz\uparrow} + [\Delta]_{yz\downarrow}^{yz\uparrow} + [\Delta]_{xy\downarrow}^{xy\uparrow})$	1	T	S	A_{1g}

where we have included for simplicity only the dominant intraorbital susceptibilities; see SM [31]. This demonstrates that spin fluctuations can induce onsite attraction in the regime $J/U < \frac{1}{3}$, where the bare interaction is repulsive. Importantly, however, this onsite channel is still substantially weaker than (nonlocal) channels driven by spin-fluctuation finite-momentum pair scattering processes, as is evident from Fig. 2(c)–2(e) [42].

IV. DISCUSSION AND CONCLUSIONS

Interorbital pair states are candidates for the superconducting ground state of many materials [13–26]. We have discussed the stability of such states within two different, widely used methods for superconducting pairing. For non-nested band structures with finite SOC, onsite Hund's pairing at the mean-field level agrees well with spin-fluctuation mediated pairing in the large-J region. By contrast, for correlated materials with bands exhibiting some degree of finite-momentum nesting, pronounced susceptibility contributions remain important, from small J up to and including

inside much of the large-J Hund's regime, and can lead to qualitatively different gap structures as seen, e.g., from comparing Figs. 2(e) and 2(g). This is relevant even though fluctuations enhance the Hund's regime for purely local pairing. We have discussed the latter findings for a band structure relevant for Sr_2RuO_4, but the results are expected to remain valid for generic bands with some degree of finite-momentum nesting including, e.g., iron-based superconductors. Our calculations therefore serve as a cautionary note against the indiscriminate application of the Hund's pairing approach and suggest that, in most unconventional superconductors of current interest, orbital-singlet, spin-triplet states of this type are not realized.

ACKNOWLEDGMENTS

[1] W. Kohn and J. M. Luttinger, New Mechanism for Superconductivity, Phys. Rev. Lett. **15**, 524 (1965).

[2] N. F. Berk and J. R. Schrieffer, Effect of Ferromagnetic Spin Correlations on Superconductivity, Phys. Rev. Lett. **17**, 433 (1966).

[3] D. Fay and A. Layzer, Superfluidity of Low-Density Fermion Systems, Phys. Rev. Lett. **20**, 187 (1968).

[4] D. J. Scalapino, E. Loh, and J. E. Hirsch, d-wave pairing near a spin-density-wave instability, Phys. Rev. B **34**, 8190 (1986).

[5] D. J. Scalapino, Superconductivity and spin fluctuations, J. Low Temp. Phys. **117**, 179 (1999).

[6] K. Miyake, S. Schmitt-Rink, and C. M. Varma, Spin-fluctuation-mediated even-parity pairing in heavy-fermion superconductors, Phys. Rev. B **34**, 6554 (1986).

[7] S. Maiti and A. V. Chubukov, Superconductivity from repulsive interaction, in *Lectures on the Physics of Strongly Correlated Systems XVII: Seventeenth Training Course in the Physics of Strongly Correlated Systems, 1–12 October 2012, Vietri sul Mare (Salerno), Italy*, edited by A. Avella and F. Mancini, AIP Conf. Proc. No. 1550 (AIP, New York, 2013), p. 3.

[8] A. T. Rømer, T. A. Maier, A. Kreisel, I. Eremin, P. J. Hirschfeld, and B. M. Andersen, Pairing in the two-dimensional Hubbard model from weak to strong coupling, Phys. Rev. Research **2**, 013108 (2020).

[9] D. J. Scalapino, A common thread: The pairing interaction for unconventional superconductors, Rev. Mod. Phys. **84**, 1383 (2012).

[10] P. J. Hirschfeld, M. M. Korshunov, and I. I. Mazin, Gap symmetry and structure of Fe-based superconductors, Rep. Prog. Phys. **74**, 124508 (2011).

[11] A. Chubukov, Pairing mechanism in Fe-based superconductors, Annu. Rev. Condens. Matter Phys. **3**, 57 (2012).

[12] A. Kreisel, P. J. Hirschfeld, and B. M. Andersen, On the remarkable superconductivity of FeSe and its close cousins, Symmetry **12**, 1402 (2020).

[13] J. Spałek, Spin-triplet superconducting pairing due to local Hund's rule and Dirac exchange, Phys. Rev. B **63**, 104513 (2001).

[14] J. E. Han, Spin-triplet s-wave local pairing induced by Hund's rule coupling, Phys. Rev. B **70**, 054513 (2004).

[15] M. Zegrodnik, J. Bünemann, and J. Spałek, Even-parity spin-triplet pairing by purely repulsive interactions for orbitally degenerate correlated fermions, New J. Phys. **16**, 033001 (2014).

[16] S. Hoshino and P. Werner, Superconductivity from Emerging Magnetic Moments, Phys. Rev. Lett. **115**, 247001 (2015).

[17] K. Kubo, Pairing symmetry in a two-orbital Hubbard model on a square lattice, Phys. Rev. B **75**, 224509 (2007).

[18] C. M. Puetter and H.-Y. Kee, Identifying spin-triplet pairing in spin-orbit coupled multi-band superconductors, Europhys. Lett. **98**, 27010 (2012).

[19] H. G. Suh, H. Menke, P. M. R. Brydon, C. Timm, A. Ramires, and D. F. Agterberg, Stabilizing even-parity chiral superconductivity in Sr_2RuO_4, Phys. Rev. Research **2**, 032023(R) (2020).

[20] J. Clepkens, A. W. Lindquist, X. Liu, and H.-Y. Kee, Higher angular momentum pairings in interorbital shadowed-triplet superconductors: Application to Sr_2RuO_4, Phys. Rev. B **104**, 104512 (2021).

[21] P. A. Lee and X.-G. Wen, Spin-triplet p-wave pairing in a three-orbital model for iron pnictide superconductors, Phys. Rev. B **78**, 144517 (2008).

[22] X. Dai, Z. Fang, Y. Zhou, and F.-C. Zhang, Even Parity, Orbital Singlet, and Spin Triplet Pairing for Superconducting $LaFeAsO_{1-x}F_x$, Phys. Rev. Lett. **101**, 057008 (2008).

[23] O. Vafek and A. V. Chubukov, Hund Interaction, Spin-Orbit Coupling, and the Mechanism of Superconductivity in Strongly Hole-Doped Iron Pnictides, Phys. Rev. Lett. **118**, 087003 (2017).

[24] J. Böker, P. A. Volkov, P. J. Hirschfeld, and I. Eremin, Quasiparticle interference and symmetry of superconducting order parameter in strongly electron-doped iron-based superconductors, New J. Phys. **21**, 083021 (2019).

[25] A. K. C. Cheung and D. F. Agterberg, Superconductivity in the presence of spin-orbit interactions stabilized by Hund coupling, Phys. Rev. B **99**, 024516 (2019).

[26] S. Sakai, R. Arita, and H. Aoki, Numerical algorithm for the double-orbital Hubbard model: Hund-coupled pairing symmetry in the doped case, Phys. Rev. B **70**, 172504 (2004).

[27] A. T. Rømer, T. A. Maier, A. Kreisel, P. J. Hirschfeld, and B. M. Andersen, Leading superconducting instabilities in three-dimensional models for Sr_2RuO_4, Phys. Rev. Research **4**, 033011 (2022).

[28] S. Cobo, F. Ahn, I. Eremin, and A. Akbari, Anisotropic spin fluctuations in Sr_2RuO_4: Role of spin-orbit coupling and induced strain, Phys. Rev. B **94**, 224507 (2016).

[29] A. T. Rømer, D. D. Scherer, I. M. Eremin, P. J. Hirschfeld, and B. M. Andersen, Knight shift and leading superconducting instability from spin fluctuations in Sr_2RuO_4, Phys. Rev. Lett. **123**, 247001 (2019).

[30] O. Gingras, R. Nourafkan, A.-M. S. Tremblay, and M. Côté, Superconducting Symmetries of Sr_2RuO_4 from First-Principles Electronic Structure, Phys. Rev. Lett. **123**, 217005 (2019).

[31] See Supplemental Material at http://link.aps.org/supplemental/10.1103/PhysRevB.106.L100501 for (i) additional details about the self-consistent pairing calculations in orbital space, (ii) derivation of the multi-orbital spin-fluctuation pairing vertex, and (iii) additional parameter-dependence of the results presented in Figs. 1 and 2 of the main text.

[32] A. T. Rømer, A. Kreisel, I. Eremin, M. A. Malakhov, T. A. Maier, P. J. Hirschfeld, and B. M. Andersen, Pairing symmetry of the one-band Hubbard model in the paramagnetic weak-coupling limit: A numerical RPA study, Phys. Rev. B **92**, 104505 (2015).

[33] A. T. Rømer, P. J. Hirschfeld, and B. M. Andersen, Superconducting state of Sr_2RuO_4 in the presence of longer-range Coulomb interactions, Phys. Rev. B **104**, 064507 (2021).

[34] A. Ramires and M. Sigrist, Superconducting order parameter of Sr_2RuO_4: A microscopic perspective, Phys. Rev. B **100**, 104501 (2019).

[35] S.-O. Kaba and D. Sénéchal, Group-theoretical classification of superconducting states of strontium ruthenate, Phys. Rev. B **100**, 214507 (2019).

[36] W. Huang, Y. Zhou, and H. Yao, Exotic cooper pairing in multiorbital models of Sr_2RuO_4, Phys. Rev. B **100**, 134506 (2019).

[37] Note that for the particular case of Sr_2RuO_4 this amounts to assuming unphysically large Hund's exchange: Constrained RPA calculations find $J/U \simeq 0.1$–0.2 [38–40]; we nevertheless evaluate the model for large J in order to discuss Hund's pairing states.

[38] J. Mravlje, M. Aichhorn, T. Miyake, K. Haule, G. Kotliar, and A. Georges, Coherence-Incoherence Crossover and the Mass-Renormalization Puzzles in Sr_2RuO_4, Phys. Rev. Lett. **106**, 096401 (2011).

[39] L. Vaugier, H. Jiang, and S. Biermann, Hubbard U and Hund exchange J in transition metal oxides: Screening versus localization trends from constrained random phase approximation, Phys. Rev. B **86**, 165105 (2012).

[40] T. Miyake, K. Nakamura, R. Arita, and M. Imada, Comparison of ab initio low-energy models for LaFePO, LaFeAsO, $BaFe_2As_2$, LiFeAs, FeSe, and FeTe: Electron correlation and covalency, J. Phys. Soc. Jpn. **79**, 044705 (2010).

[41] For larger values of λ_{so}, the order parameters in orbital and spin space become qualitatively similar at lower values of J/U when comparing Hund's pairing vs spin-fluctuation pairing, but mean-field Hund's pairing still produce significantly lower T_c values.

[42] For ferromagnetic fluctuations the renormalization of the onsite channel should more reliably capture changes to the pairing vertex from spin fluctuations.